Journal of Vibration Engineering & Technologies (2018) 6:483–494
https://doi.org/10.1007/s42417-018-0065-9

ORIGINAL PAPER

Free Vibration Analysis of Functionally Graded Shaft System with a Surface Crack

Debabrata Gayen[1] · **Debabrata Chakraborty**[1] · **Rajiv Tiwari**[1]

Received: 12 January 2017 / Revised: 19 January 2017 / Accepted: 25 January 2017 / Published online: 29 November 2018

Abstract

Background Free vibration analysis of functionally graded (FG) non-spinning simply supported shaft having a transverse surface crack has been carried out. Material properties of the FG shaft are assumed to be graded radially following the power law of material gradation.

Method Local flexibility coefficients as a function of depth of crack are computed with the help of Paris' equation along with Castigliano's theorem. Finite element (FE) formulation has been done using Timoshenko beam elements with two nodes and having four degrees of freedom per node. Based on the formulation, FE analysis has been performed to understand the effects of shaft's slenderness, crack's depth and location, gradient parameter and thermal gradient on the free vibration response of the cracked FG shaft.

Results FE analysis show that for a cracked FG shaft, both gradation parameter and crack parameters have significant influence on the free vibration response.

Conclusions Gradation parameter could be suitably chosen in the design of FG shafts so as to minimize the increase in flexibility due to appearance of cracks.

Keywords Functionally graded material · Material gradient index · Flexibility coefficient · Cracked shaft · Temperature effects

Introduction

Functionally graded materials (FGMs) are advanced classes of nonhomogeneous materials having advantages over conventional metallic materials and laminated composites, especially in high temperature applications. The first FGM concept was proposed in 1984 by Niino et al. at the National Aerospace Laboratory of Japan [1, 2]. Limitations of layered laminated composite shaft, such as thermomechanical property mismatch and inter-laminar stresses could be reduced by the use of FG shafts in design of rotating machinery components. Some works are already available in existing literatures dealing with structures made of FGMs [3–7] along with a few works on FG shafts. Studies on parametric instability of FG beams subjected to a periodic load are also reported along with the effects of system parameters on instability [8, 9]. Gayen and Roy [10] reported the FE-based stability analysis of a rotating FG shaft.

Studying the influence of crack is very important, as the presence of crack may lead to structural failure sometimes associated with loss of economic and human life. Exhaustive literature reviews [11] have been reported which provided valuable information and knowledge about the vibration of cracked structures. A number of works [12, 13] has been reported where local flexibility matrixes are derived for cracked structures. Sekhar and Prabhu [14] have presented the vibration studies of cracked shaft along with identification and detection of crack. The dynamic analysis and influence of crack parameters on homogeneous structural members have been reported by Sinou and Lees [15]. Darpe et al. [16] reported analytical solutions of cracked rotor and obtained various dynamic responses with the surface crack and breathing crack conditions.

✉ Debabrata Chakraborty
chakra@iitg.ac.in

Debabrata Gayen
d.gayen@iitg.ac.in

Rajiv Tiwari
rtiwai@iitg.ac.in

[1] Mechanical Engineering Department, Indian Institute of Technology Guwahati, Guwahati, Assam 781039, India

Theoretical studies of free vibration and buckling responses for FG cracked beam were presented by Yang and Chen [17]. Ke et al. [18] analytically solved buckling and vibration problem for FG beams. Free vibrations of a cracked FG beam were performed analytically by Ferezqi et al. [19]. Wei et al. [20] analytically solved vibration problem of cracked beams made of FGM with multiple cracks. Aydin [21] studied the effects of crack's depth and location, material gradient and end conditions on natural frequency of cracked beam made of FGMs.

From the literature review, it could be seen that a good number of published literatures are available in the analysis of structures made of FGM and in addition a few works are also available on FG shafts. However, works on the analysis of cracked FG shafts are scanty even though there are a few works available for such FG beams. Due to its increasing potential demands in various important engineering sections, it is important to analyze transverse vibration of cracked FG shafts. Thus, in this work an attempt is made to develop an FE model capable of analyzing free vibration of cracked FG shaft and to understand the influences of crack's depth and location, slenderness ratio, material gradient parameter and thermal gradient on free vibration of the shaft.

Table 1 Mechanical properties of composition of FGM

Properties	Steel	Al_2O_3
E (GPa)	210	390
ρ (kg/m^3)	7800	3960
ν	0.3	0.26

FE Modeling of an FG Cracked Shaft

Timoshenko beam elements have been used for modeling the non-spinning FG shaft with simply supported end conditions where the properties of material are graded radially. Each element has two nodes and four degrees of freedom at each node. A transverse surface crack is considered and crack is assumed as open. Transverse vibration is studied where damping is not considered. Figure 1a–c shows the FE model of the shaft, a shaft element along with general loads and the cracked cross-section geometry, respectively. Here, the total length is L, L_e is the element length and α is the crack depth at distance L_c from the left end support of the shaft. The shaft element is loaded with bending moments P_4, P_5, P_{10} and P_{11}, shear forces P_2, P_3, P_8 and P_9. R and b are the shaft radius and half-width of the crack, respectively.

In presence of crack on FG shaft, local flexibility coefficients (LFCs) are derived by applying Paris' equation [22] in Castigliano's theorem where stress intensity factors (SIFs) are expressed as [12].

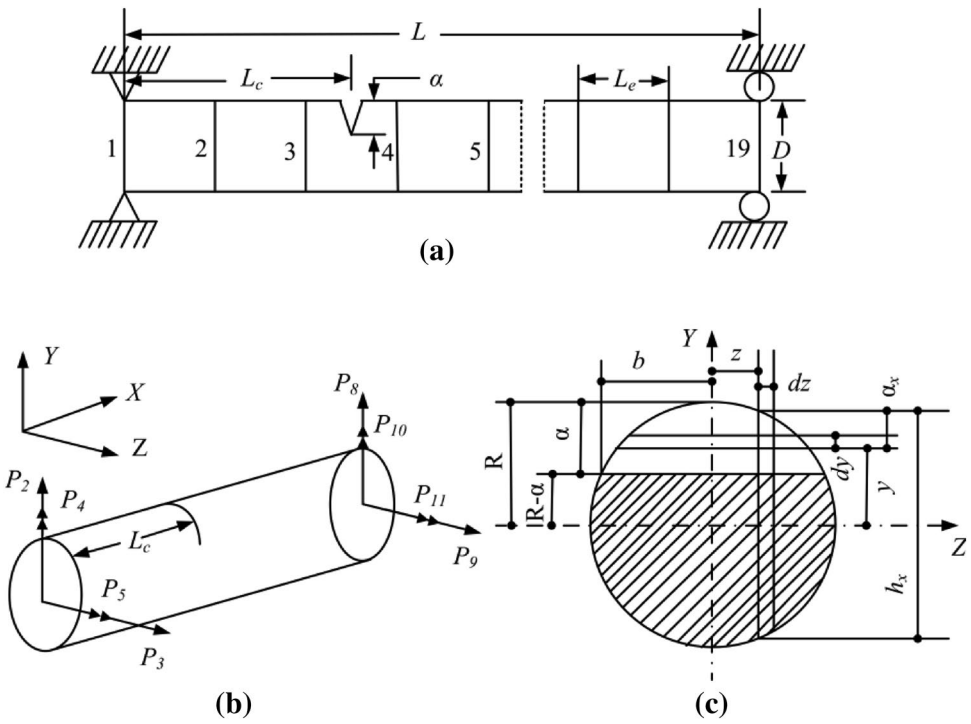

Fig. 1 FG cracked shaft: **a** finite element discretization, **b** shaft element, **c** cracked cross-section geometry

Table 2 Temperature coefficients for mechanical properties [3]

Coefficient	E (Pa)		K (W/m K)	
	SS	Al_2O_3	SS	Al_2O_3
C_0	201.0354×10^9	349.5486×10^9	15.37895	−14.087
C_{-1}	0	0	0	−1123.6
C_1	3.079296×10^{-4}	-3.853206×10^{-4}	−0.001264	0.00044
C_2	-6.533971×10^{-7}	4.026993×10^{-7}	0.20923×10^{-5}	0
C_3	0	-1.6734×10^{-10}	-0.0722×10^{-8}	0

Table 3 Dimensionless compliance $\overline{C}_{55}$ with α/R

$\left(\frac{\alpha}{R}\right)$	$\overline{C}_{55}$	
	Papadopoulos [13]	Present
0.12	0.043041	0.0430410
0.20	0.144614	0.1446141
0.36	0.567780	0.5677802
0.44	0.904893	0.9048936
0.52	1.340520	1.3405230
0.60	1.892200	1.8922033
0.76	3.456030	3.4560272
0.84	4.556690	4.5566926
0.92	5.963420	5.9634219
1.00	7.790390	7.7903871

In the presence of crack, strain energy U_c and displacement u_i^c are expressed as,

$$u_i^c = \frac{\partial U_c}{\partial P_i}, \quad U_c = \int_0^{\alpha_x} J(y)\,\mathrm{d}y$$

$$\text{and} \quad J(y) = \frac{1}{E(y,T)}\left[\left(\sum_{i=2}^{5} K_{Ii}\right)^2 + \left(\sum_{i=2}^{5} K_{IIi}\right)^2 + \{1+\nu(y)\}\left(\sum_{i=2}^{5} K_{IIIi}\right)^2\right], \tag{1}$$

where strain energy release rate $J(y)$ is a function of geometry of crack and loads applied, $E(y,T)$ is Young's modulus, Poisson ratio is $\nu(y)$. K_I, K_{II} and K_{III} are mode I, II and III SIFs, respectively and $i = 2, 3, 4, 5$ are load indices. Referring to Fig. 1c, finally the cracked shaft direct and cross-couple LFCs are computed as

$$C_{ij}^c = \frac{\partial u_i^c}{\partial P_j} = \frac{\partial^2}{\partial P_i\,\partial P_j}\int_{-b}^{b}\int_0^{\alpha_x} J(y)\,\mathrm{d}y\mathrm{d}z, \tag{2}$$

where $\alpha_x = (\alpha - R) + \sqrt{R^2 - z^2}$ and $b = \sqrt{R^2 - (R-\alpha)^2}$.

Table 4 Natural frequencies (in Hz) of simply supported, homogenous, un-cracked shaft

Modes	Metal (steel) shaft		Ceramic (Al_2O_3) shaft	
	Theoretical	Present	Theoretical	Present
1st	163.009	162.688	311.770	311.156
2nd	163.009	162.688	311.770	311.156
3rd	652.036	646.954	1247.080	1237.359
4th	652.036	646.954	1247.080	1237.359

While performing the integrations in Eq. (2) for determination of the direct and cross-couple terms of LFCs, $E(y,T)$ and $\nu(y)$ are considered temperature dependent as well as function of radial direction.

In the presence of crack, the local flexibility matrix C^c is represented as

$$C^c = \begin{bmatrix} C_{22}^c & 0 & 0 & 0 \\ 0 & C_{33}^c & 0 & 0 \\ 0 & 0 & C_{44}^c & C_{45}^c \\ 0 & 0 & C_{45}^c & C_{55}^c \end{bmatrix}. \tag{3}$$

The elements of C^c are given in detail in Appendix A. Total flexibility matrix is given as

$$C = C^{uc} + C^c, \tag{4}$$

where C^{uc} is the un-cracked flexibility matrix obtained using energy method as

$$C^{uc} = \frac{L_e}{6E(y,T)I}\begin{bmatrix} 2L_e^2 & 0 & 0 & 3L_e \\ 0 & 2L_e^2 & -3L_e & 0 \\ 0 & -3L_e & 6 & 0 \\ 3L_e & 0 & 0 & 6 \end{bmatrix}, \tag{5}$$

where I denotes area moment of inertia.

From the conditions of equilibrium of shaft element,

$$\{P_2, P_8, P_3, P_9, P_4, P_{10}, P_5, P_{11}\}^T = \mathbf{\Pi}^T \{P_8, P_9, P_{10}, P_{11}\}^T, \tag{6}$$

where the transformation matrix is

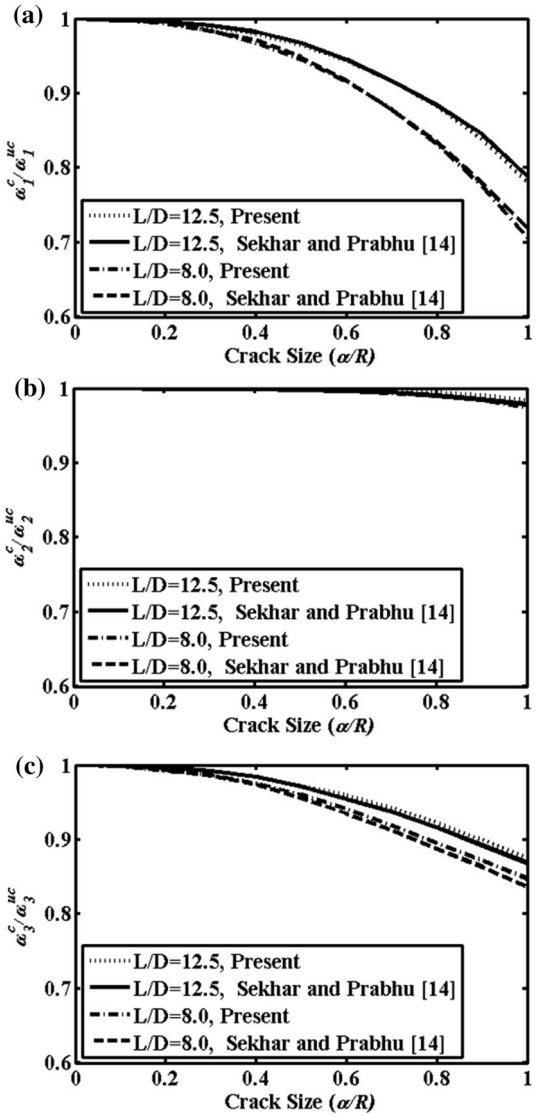

Fig. 2 Variation of $\omega_i^{\mathrm{c}}/\omega_i^{\mathrm{uc}}$ with α/R and L/D: **a** first, **b** second, **c** third

$$\Pi = \begin{bmatrix} -1 & 1 & 0 & 0 & 0 & 0 & -L_{\mathrm{e}} & 0 \\ 0 & 0 & -1 & 1 & L_{\mathrm{e}} & 0 & 0 & 0 \\ 0 & 0 & 0 & 0 & -1 & 1 & 0 & 0 \\ 0 & 0 & 0 & 0 & 0 & 0 & -1 & 1 \end{bmatrix}.$$

For the cracked element, the stiffness matrix is derived applying the virtual work principle as

$$K_{\mathrm{c}} = \Pi^{\mathrm{T}} C^{-1} \Pi. \tag{7}$$

System Equation of Motion

Having a crack on the FG shaft in fixed coordinate, the system equations of motion are

$$\mathbf{M}\ddot{\mathbf{p}}(t)+\mathbf{K}\mathbf{p}(t)= \mathbf{f}(t), \tag{8}$$

where $\mathbf{M}$ represents the rotary and translational mass matrix, $\mathbf{K}$ represents the structural stiffness matrix and the vectors of nodal displacement and external forces are presented by $\mathbf{p}(t)$ and $\mathbf{f}(t)$, respectively.

Material Property Variation of FGMs

In thermal environment, material properties C [23] are considered as

$$C = C_0(C_{-1}T^{-1} + 1 + C_1T + C_2T^2 + C_3T^3), \tag{9}$$

where temperature (T in Kelvin) coefficients for each constituent material is presented by C_0, C_{-1}, C_1,C_2 and C_3.

According to the power law gradation, material properties $C(y, T)$ vary with radial coordinate and temperature [4] as

$$C(y,T) = C_{\mathrm{m}}(T) + \{C_{\mathrm{c}}(T) - C_{\mathrm{m}}(T)\}\left(\frac{y - R_{\mathrm{m}}}{R_{\mathrm{c}} - R_{\mathrm{m}}}\right)^k, \tag{10}$$

where C represents the properties [E, ν K (thermal conductivity) and ρ (density)]. m and c represent subscripts for metal and ceramic, respectively. For fully ceramic material gradient index $k \to 0$ and for fully metal $k \to \infty$.

Temperature distribution obtained in the radially graded FG shaft using Fourier equation of heat conduction (steady-state one-dimensional) without heat generation is,

$$\frac{\mathrm{d}}{\mathrm{d}y}\left[K(y)\frac{\mathrm{d}T}{\mathrm{d}y}\right] = 0, \tag{11}$$

where at $y = R_{\mathrm{m}}, T = T_{\mathrm{m}}$ and at $y = R_{\mathrm{c}}, T = T_{\mathrm{c}}$. The solution of Eq. (11) was obtained following [5] as,

$$T(y) = T_{\mathrm{m}} + (T_{\mathrm{c}} - T_{\mathrm{m}})\zeta(y). \tag{12}$$

Solution Procedure

For cracked elements, the element stiffness matrix is replaced by K_{c} in the global stiffness matrix K. Thus, eigen frequencies are computed by solving for eigenvalue of $K - \omega_i^{\mathrm{uc}2} M = 0$ and $K_{\mathrm{c}} - \omega_i^{\mathrm{c}2} M = 0$, for the un-cracked and cracked shaft system, respectively. ω_i^{c} and ω_i^{uc} are natural frequencies for FG cracked and un-cracked shaft, respectively, and the mode number indicates by i.

Results and Discussions

Using the formulation discussed in "FE Modeling of an FG Cracked Shaft", a finite element code is developed in MATLAB environment. Aluminum oxide (Al_2O_3) and

Table 5 Variation in dimensionless frequencies for a FG cracked beam with end conditions

E_2/E_1	Cantilever		
	Present	Yang and Chen [17]	Wei et al. [20]
0.2	0.9748	0.9811	0.9755
1.0	0.9956	0.9951	0.9921
5.0	0.9983	0.9986	0.9949
E_2/E_1	Simply supported		
	Present	Yang and Chen [17]	Wei et al. [20]
0.2	0.9376	0.9535	0.9501
1.0	0.9890	0.9912	0.9874
5.0	0.9956	0.9992	0.9985
E_2/E_1	Fixed–fixed		
	Present	Yang and Chen [17]	Wei et al. [20]
0.2	0.9867	0.9871	0.9855
1.0	0.9971	0.9966	0.9954
5.0	0.9988	0.9990	0.9987

steel are considered to form the FGM. Material properties for steel, stainless steel (SS) and aluminum oxide are listed in Tables 1 and 2. A shaft (both the homogeneous as well as the FG shaft) with simply supported boundary conditions is modeled using 19 elements as shown in Fig. 1a. In this study, shaft diameter, $D = 0.08$ m and slenderness ratio $L/D = 12.5, 11.5, 10.5$ are considered.

Validation of the FE Code for Homogeneous Material

For validation, a shaft with $L = 1$ m, $D = 0.08$ m and made of steel is considered. The compliance $\overline{C}_{55}$ in dimensionless form determined with crack size α/R and Table 3 shows an excellent agreement when compared with published results [13]. The code has also been validated by showing excellent agreements while comparing the natural frequencies obtained with those obtained from closed form solutions for the metal and ceramic shafts, as shown in Table 4.

The first four dimensionless natural frequencies (ω_i^c/ω_i^{uc}) with α/R and L/D, are computed for centrally located crack, and compared with published work by Sekhar and Prabhu [14] for cracked metal shaft as shown in Fig. 2a–c and an excellent agreement could be observed.

Validation of the FE Code for Cracked FG Beam

After validating the FE formulation for homogenous cracked shaft, the code has also been validated for a cracked FG component. In the absence of numerical results for a cracked FG shaft, validation has been done by comparing the results obtained from the present code for a cracked FG beam with the already published results [17, 20].

For this, a cracked FG beam with different end conditions (cantilever, simply supported, fixed–fixed), and with dimensions ($L/D = 10.0, \alpha/R = 0.4, k = 2.0$) and material properties ($E_1 = 70$ GPa, $\rho_1 = 2780$ kg/m^3, $\nu = 0.33$) similar to those used by Yang and Chen [17] and Wei et al. [20] are used. Computed dimensionless natural frequencies are compared with published analytical solutions [17, 20] and are tabulated in Table 5. It shows an excellent agreement with those of published results thus validating the developed code.

Variation of LFCs with α/R and k

In the presence of crack on FG shaft, dimensionless direct and cross-couple LFCs are determined as $\overline{C}_{22} = C_{22}/\pi E_m R$, $\overline{C}_{33} = C_{33}/\pi E_m R$, $\overline{C}_{44} = C_{44}/\pi E_m R^3$, $\overline{C}_{45} = C_{45}/\pi E_m R^3$, $\bar{C}_{55} = C_{55}/\pi E_m R^3$. Variations of dimensionless LFCs with α/R and different material gradient indices k have been plotted in Fig. 3a–e. It could be observed from Fig. 3a–e that as α/R increases dimensionless LFCs increase and for a given α/R, as k increases the LFCs increase. This is because the metal content increases as k increase.

Variation in ω_i^c with α/R

First four natural frequencies are determined for cracked FG (steel/Al_2O_3) and metal (steel) shafts with $k = 0.5$ and

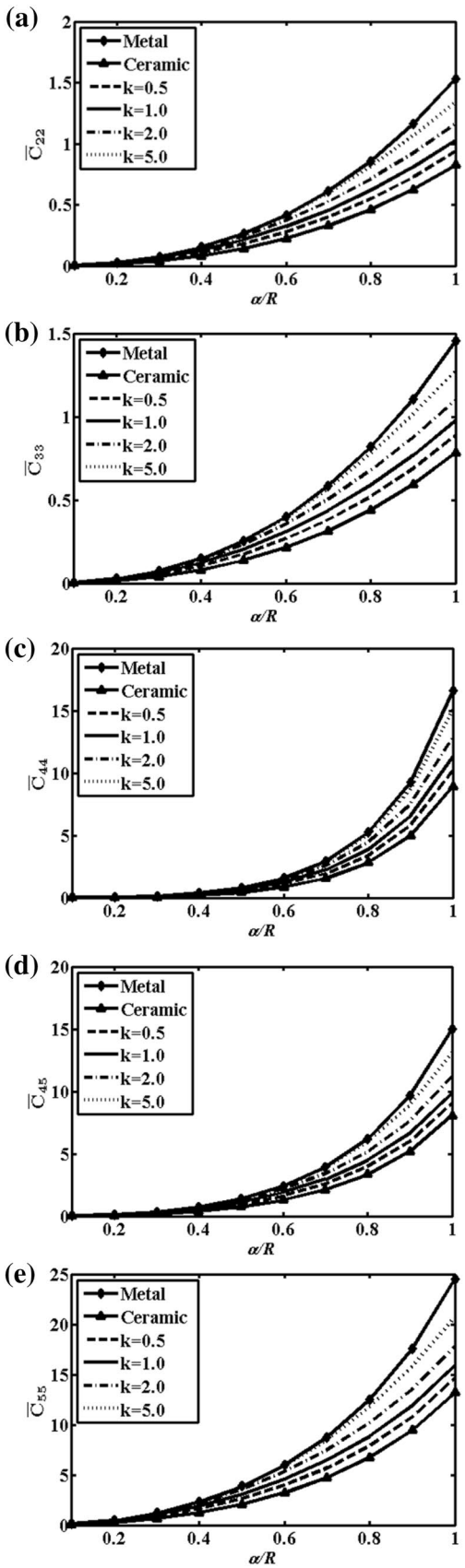

Fig. 3 Variation of LFCs. **a** $\overline{C}_{22}$, **b** $\overline{C}_{33}$, **c** $\overline{C}_{44}$, **d** $\overline{C}_{45}$ and **e** $\overline{C}_{55}$ with α/R for different k

$L/D = 12.5$, and for different α/R and are listed in Table 6. Results in Table 6 show that for each mode, the natural frequency of shaft made of FGM is more compared to that of the metallic shaft and the frequencies are higher for the un-cracked shaft than those for the cracked shaft. Results also show that for a specific L/D, crack location L_c/L and k as α/R increases, natural frequencies decrease for all the modes. However, for the first and third mode, the percentage reduction in frequency is observed to be higher than those for the second and fourth modes. This is due to the fact that mode shapes for first and third modes are anti-nodes at the crack location. It is also noticed that the extent of percentage reduction in frequency is higher in the FG shaft than those of the homogeneous (metal) shaft.

Effect of α/R and k on ω_i^c

For the FG shaft system having $L/D = 12.5$ and $L_c/L = 0.5$, Fig. 4a–d shows the variations of first four frequencies with k and α/R. From Fig. 4a–d, it is clearly noticed that with increase in α/R, natural frequencies decreases and at particular values of α/R, natural frequencies increase with decrease in k. It could be also seen that at higher values of α/R reduction in natural frequency with α/R is more compared to that for lower α/R. It is observed that for all the four modes, variations in natural frequencies are more for $k < 1$, which represents increase in ceramic content.

Effect of α/R and L_c/L on Natural Frequency

With a crack on an FG shaft with $k = 3.0$ and $L/D = 12.5$, Fig. 5a–d shows the first four dimensionless natural frequencies corresponding to different values of α/R and L_c/L. Results show that for a given L/D, α/R and k, the first four natural frequencies (dimensionless) monotonically decrease as α/R increase and the extent of reduction in natural frequency is maximum for the first mode and is minimum for the third mode. However, for an offset crack located at $L_c/L = 0.1316$, reduction in the natural frequency is maximum for third mode and is minimum for first mode.

Figure 6a–d shows the variation in first four natural frequencies (dimensionless) with crack locations and k, for $L/D = 12.5$ and $\alpha/R = 0.6$, it is seen that increase in k leads to more reduction in all the modes. However, the amount of reduction is dependent on the crack location.

Table 6 Variation in natural frequencies (in Hz) with α/R for homogeneous (steel) and FG (steel/Al_2O_3) shaft

Modes	Un-cracked	Crack size α/R			
		FG (steel/Al_2O_3) shaft, $k = 0.5$			
		0.2	0.4	0.6	0.8
First	255.92	241.87	203.46	161.00	123.19
Second	255.92	255.61	252.66	242.83	220.57
Third	1017.71	1015.98	1011.09	1005.34	999.61
Fourth	1017.71	1017.46	1016.28	1013.53	1008.53
Modes	Un-cracked	Cracked metal (steel) shaft			
		0.2	0.4	0.6	0.8
First	162.68	155.48	132.66	104.78	78.98
Second	162.68	162.53	160.92	155.11	140.97
Third	646.95	646.06	643.17	639.44	635.58
Fourth	646.95	646.83	646.17	644.51	641.29

Effect of α/R and L/D on Natural Frequency

Figure 7a–d shows the first four natural frequencies ω_i^c for a cracked FG shaft with $k = 3.0$ and $L_c/L = 0.5$ for different L/D and α/R. These results show that for a given $L/D, L_c/L$ and k, ω_i^c decrease with the increase in α/R. However, for first and third modes, the reductions are observed to be more than those for the second and fourth modes. It also shows for the cracked shaft that ω_i^c increases as L/D decreases. Results in Table 7 show that with decrease in L/D, natural frequencies increase and in the presence of crack, percentage increase in natural frequencies with decreasing L/D is more as compared to that of un-cracked FG shaft.

Effect of Temperature Gradient on Natural Frequency

Table 8 shows the first four natural frequencies for cracked FG (SS/Al_2O_3) shaft system considering temperature-dependent material properties (Table 2) for different α/R and temperature gradient ΔT, with $k = 0.5$, $L/D = 12.5$ and $L_c/L = 0.5$. Further, with the variation of L_c/L and temperature gradient, for $\alpha/R, k = 0.5$ and $L/D = 12.5$, results are tabulated in Table 9. Results from both Tables 8 and 9 show that temperature has little effect on natural frequencies for lower α/R and L_c/L but for higher values of α/R and L_c/L, natural frequencies are observed to decrease, while ΔT increases. This is because the material becomes softer at higher values of ΔT.

Influence of End Conditions on ω_1^c

To understand the importance of end conditions on ω_1^c of the shaft made of FGM, cantilever, simply supported and fixed–fixed are considered for the a non-spinning shaft made of FGM and frequency with $k, L_c/L$, for $\alpha/R = 0.6$ and $L/D = 12.5$ are computed using the present code and listed in Table 10. As expected for simply supported and fixed–fixed end conditions, fundamental frequency is same for symmetrically located cracks with respect to the mid span of the shaft. However, for cantilever, fundamental frequency values decrease as crack location is moved from fixed end towards the free end. In addition, for the end conditions, ω_1^c decrease with the increase in material gradient index.

Conclusions

In this work, a FE-based formulation is put forward to study the free vibration characteristics for a simply supported shaft considering transverse crack on FG shaft. Stiffness of the cracked FG shaft is modified by calculating the direct and cross-couple terms of LFCs. Using the FE code developed, the effects of crack depths, locations, slenderness ratios, temperature gradients and material gradient indices on the free vibration for the shaft made of FGM are determined. The outcomes of the present work are stated as

- In an FG shaft, where a crack is developed, LFCs are significantly influenced by the material gradient parameter for a given crack depth. Thus, by deciding a suitable material gradient index, the increase in flexibility due to the presence of a crack could be minimized.
- For a given L/D and location of crack, as crack size increase, the natural frequency decreases. This reduction in natural frequencies is dependent on material

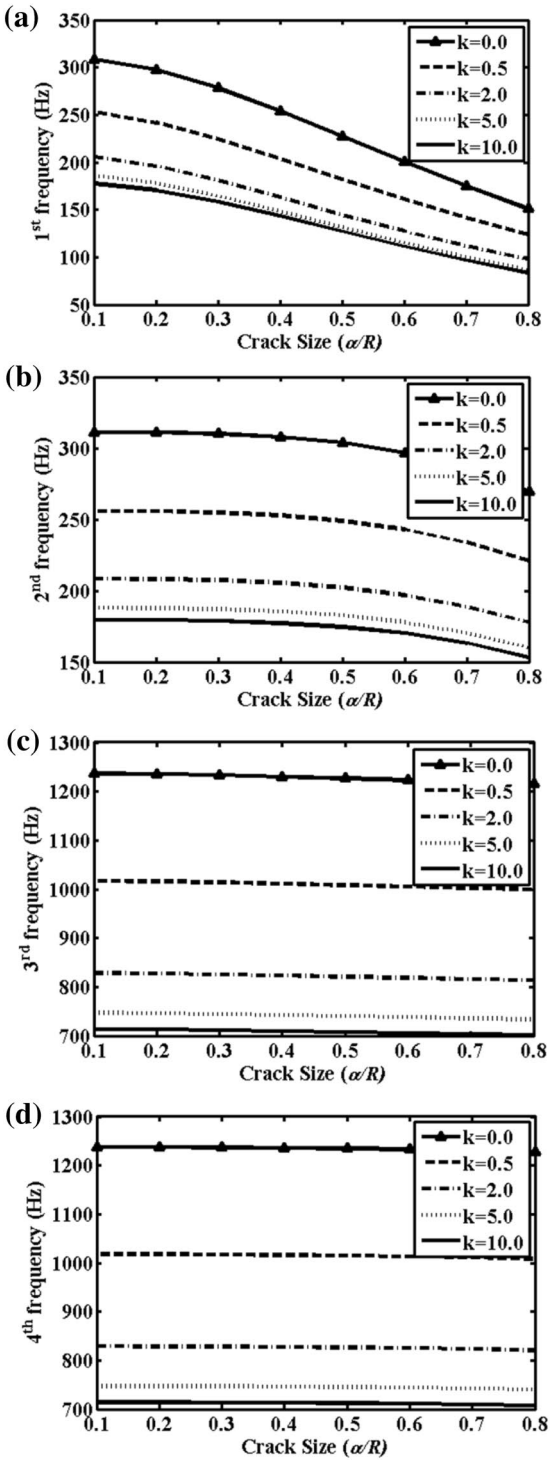

Fig. 4 Variation of ω_i^c with α/R for different k: **a** first, **b** second, **c** third and **d** fourth

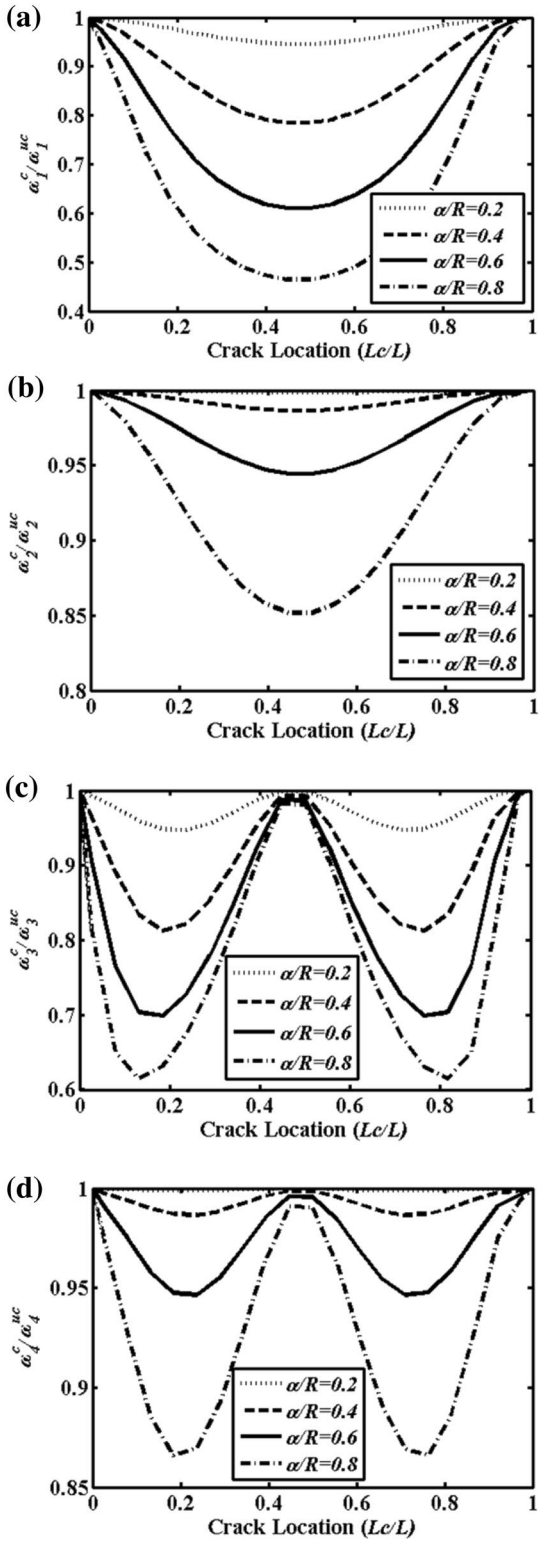

Fig. 5 Variation of ω_i^c with L_c/L and α/R: **a** first, **b** second, **c** third and **d** fourth

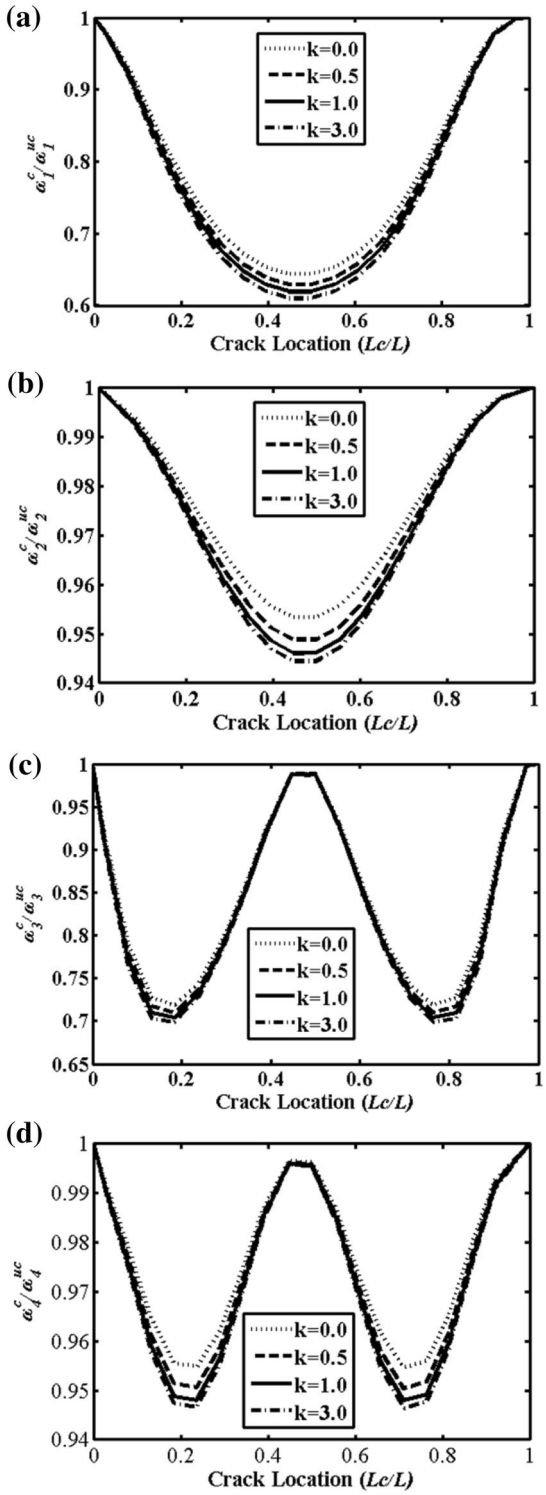

Fig. 6 Variation of ω_i^c with L_c/L and k: **a** first, **b** second, **c** third and **d** fourth

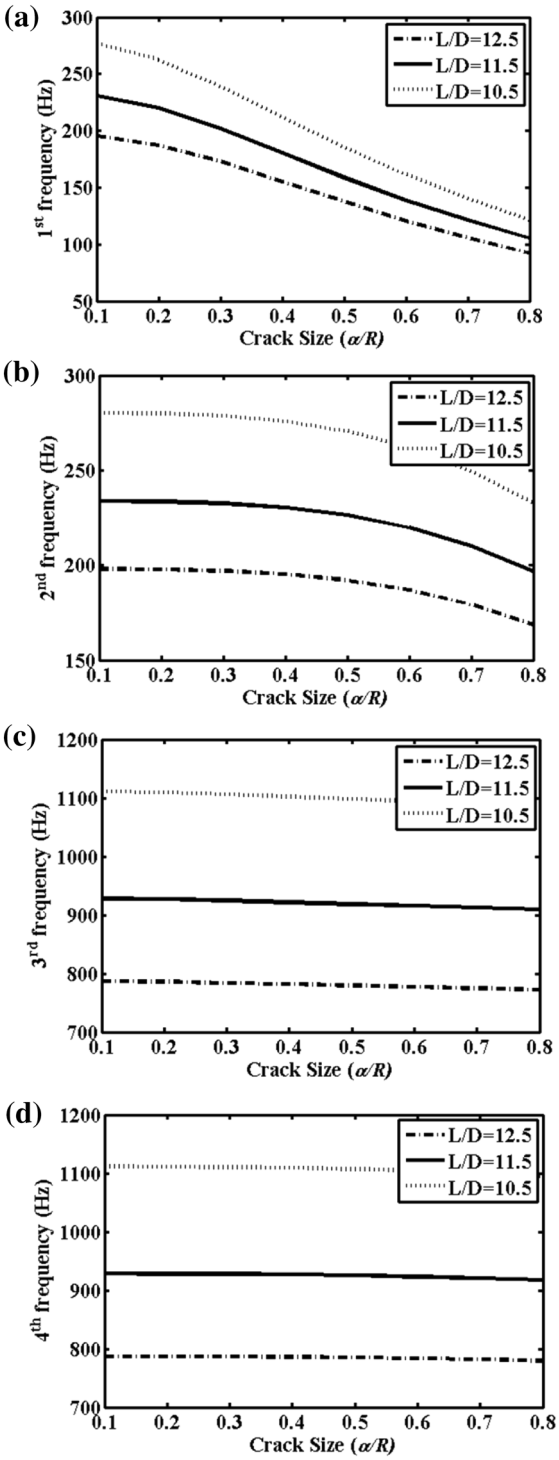

Fig. 7 Variation of ω_i^c with α/R and L/D: **a** first, **b** second, **c** third and **d** fourth

Table 7 Variation in ω_i (in Hz) with L/D

Modes	$\alpha/R = 0.6$			
	$L/D = 12.5$		$L/D = 11.5$	
	Un-cracked	Cracked	Un-cracked	Cracked
First	197.89	120.66	233.72	138.75
Second	197.89	186.90	233.72	219.71
Third	786.95	776.82	928.46	915.35
Fourth	786.95	783.40	928.46	923.37
Modes		$L/D = 10.5$		
		Un-cracked		Cracked
First		280.23		161.42
Second		280.23		261.98
Third		1111.70		1094.18
Fourth		1111.70		1104.10

Table 8 Variation in ω_i^c (in Hz) with α/R and ΔT

Modes	$\alpha/R = 0.4$		
	$\Delta T = 0$ K	$\Delta T = 300$ K	$\Delta T = 600$ K
First	189.16	187.38	187.21
Second	233.27	231.06	230.85
Third	933.13	924.27	923.46
Fourth	937.79	928.88	928.07
	$\alpha/R = 0.7$		
	$\Delta T = 0$ K	$\Delta T = 300$ K	$\Delta T = 600$ K
First	131.16	128.87	128.01
Second	215.94	212.22	210.87
Third	925.10	909.23	903.65
Fourth	933.29	917.28	911.65
	$\alpha/R = 1.0$		
	$\Delta T = 0$ K	$\Delta T = 300$ K	$\Delta T = 600$ K
First	82.81	80.76	79.33
Second	166.77	162.54	159.42
Third	916.84	893.52	876.21
Fourth	923.37	899.89	882.44

Table 9 Variation in ω_i^c (in Hz) with L_c/L and ΔT

Modes	$L_c/L = 0.1842$		
	$\Delta T = 0$ K	$\Delta T = 300$ K	$\Delta T = 600$ K
First	186.42	183.69	182.95
Second	231.33	227.96	227.09
Third	668.79	659.01	656.39
Fourth	894.64	881.60	878.19
	$L_c/L = 0.3421$		
	$\Delta T = 0$ K	$\Delta T = 300$ K	$\Delta T = 600$ K
First	156.28	153.98	153.35
Second	226.05	222.75	221.89
Third	802.36	790.66	787.61
Fourth	913.63	900.33	896.88
	$L_c/L = 0.5000$		
	$\Delta T = 0$ K	$\Delta T = 300$ K	$\Delta T = 600$ K
First	149.58	147.38	146.77
Second	224.39	221.12	220.26
Third	927.79	914.29	910.82
Fourth	935.29	921.69	918.19

Table 10 Variation in fundamental frequency (in Hz) with different end conditions and surface crack at different k and L_c/L for $\alpha/R = 0.6$

L_c/L	Cantilever			
	$k = 0.0$	$k = 0.5$	$k = 1.0$	$k = 3.0$
0.2368	75.66	60.91	54.20	45.78
0.5000	98.20	80.04	71.82	61.12
0.7632	110.20	90.58	81.76	69.98
L_c/L	Simply supported			
	$k = 0.0$	$k = 0.5$	$k = 1.0$	$k = 3.0$
0.2368	231.41	186.83	166.55	140.90
0.5000	200.40	161.00	143.06	120.66
0.7632	231.41	186.83	166.55	140.90
L_c/L	Fixed–fixed			
	$k = 0.0$	$k = 0.5$	$k = 1.0$	$k = 3.0$
0.2368	692.61	569.21	513.71	439.69
0.5000	553.83	451.45	405.24	345.12
0.7632	692.61	569.21	513.71	439.69

gradient parameter k. Thus, choosing a proper material gradient parameter may limit the extent of reduction in ω for a surface crack to appear on the FG shaft.

- For all the four modes, the studied maximum changes in natural frequency is observed corresponding to material gradient index less than 1 (one).
- Even though the natural frequency decrease with the increase in slenderness ratio, it is possible to allow higher slenderness ratio for designing an FG shaft by choosing a proper material gradient parameter.
- Temperature gradient has little effect on the variation in ω, however, with increase in crack size the reduction increases.
- Decrease in fundamental frequency with the increase in material gradient is more pronounced in case of fixed–fixed end condition compared to those in the case of simply supported and cantilever cases.

Appendix A: Local Flexibility Coefficients

The local flexibility coefficients are

$$C_{22}^{c} = \frac{4}{\pi R^4} \int_0^b \int_0^{\alpha_x} \frac{\{1+\nu(y)\}\kappa^2 y}{E(y,T)} F_{\mathrm{III}}^2\left(\frac{y}{h_x}\right) \mathrm{d}y\, \mathrm{d}z,$$

$$C_{33}^{c} = \frac{1}{\pi R^4} \int_0^b \int_0^{\alpha_x} \frac{\{1+\nu(y)\}\kappa^2 y}{E(y,T)} F_{\mathrm{II}}^2\left(\frac{y}{h_x}\right) \mathrm{d}y\, \mathrm{d}z,$$

$$C_{44}^{c} = \frac{64}{\pi R^8} \int_0^b \int_0^{\alpha_x} \frac{y}{E(y,T)} z^2 F_1^2\left(\frac{y}{h_x}\right) \mathrm{d}y\, \mathrm{d}z,$$

$$C_{55}^{c} = \frac{64}{\pi R^8} \int_0^b \int_0^{\alpha_x} \frac{y}{E(y,T)} (R^2 - z^2) F_2^2\left(\frac{y}{h_x}\right) \mathrm{d}y\, \mathrm{d}z,$$

$$C_{45}^{c} = \frac{64}{\pi R^8} \int_0^b \int_0^{\alpha_x} \frac{y}{E(y,T)} z\sqrt{R^2 - z^2}\, F_1\left(\frac{y}{h_x}\right) F_2\left(\frac{y}{h_x}\right) \mathrm{d}y\, \mathrm{d}z,$$

where F_1, F_2, F_{II} and F_{III} are form factors [22] and $h_x = 2\sqrt{R^2 - z^2}$, $\kappa = 6\{1+\nu(y)\}/\{7+6\nu(y)\}$.

References

1. Niino M, Hirai T, Watanabe R (1987) The functionally gradient materials. J Jpn Soc Compos Mater 13:254–264
2. Koizumi M (1993) The concept of FGM. Ceram Trans 34:3–10
3. Reddy JN, Chin CD (1998) Thermoelastical analysis of functionally graded cylinders and plates. J Therm Stress 21(6):593–626
4. Shen H-S (2009) Functionally graded materials nonlinear analysis of plates and shells. CRC, Taylor & Francis, Boca Raton
5. Lanhe W (2004) Thermal buckling of a simply supported moderately thick rectangular FGM plate. Compos Struct 64(2):211–218
6. Azadi M (2011) Free and forced vibration analysis of FG beam considering temperature dependency of material properties. J Mech Sci Technol 25(1):69–80
7. Piovan MT, Sampaio R (2009) A study on the dynamics of rotating beams with functionally graded properties. J Sound Vib 327(1–2):134–143
8. Kona M, Ray K (2010) Parametric instability and control of functionally graded beams. J Vib Eng Technol 9(1):105–118
9. Mohanty SC, Dash RR, Rout T (2014) Parametric instability of functionally graded Timoshenko beam in high temperature environment. J Vib Eng Technol 2(3):205–228
10. Gayen D, Roy T (2014) Finite element based vibration analysis of functionally graded spinning shaft system. J Mech Eng Sci Part C 228(18):3306–3321
11. Dimarogonas AD (1996) Vibration of cracked structures: a state of the art review. Eng Fract Mech 55(5):831–857
12. Papadopoulos CA, Dimarogonas AD (1987) Coupled longitudinal and bending vibrations of a rotating shaft with an open crack. J Sound Vib 117(1):81–93
13. Papadopoulos CA (2004) Some comments on the calculations of the local flexibility of cracked shafts. J Sound Vib 278:1205–1211
14. Sekhar AS, Prabhu BS (1992) Crack detection and vibration characteristics of cracked shafts. J Sound Vib 157(2):375–381
15. Sinou JJ, Lees AW (2005) The influence of cracks in rotating shafts. J Sound Vib 285(4–5):1015–1037
16. Darpe AK, Chawla A, Gupta K (2002) Analysis of the response of a cracked Jeffcott rotor to axial excitation. J Sound Vib 249(3):429–445
17. Yang J, Chen Y (2008) Free vibration and buckling analyses of functionally graded beams with edge cracks. Compos Struct 83(1):48–60
18. Ke LL, Yang J, Kitipornchai S, Xiang Y (2009) Flexural vibration and elastic buckling of a cracked Timoshenko beam made of functionally graded materials. Mech Adv Mater Struct 16(6):488–502
19. Ferezqi HZ, Tahani M, Toussi HE (2010) Analytical approach to free vibrations of cracked Timoshenko beams made of functionally graded materials. Mech Adv Mater Struct 17(5):353–365
20. Wei D, Liu Y, Xiang Z (2012) An analytical method for free vibration analysis of functionally graded beams with edge cracks. J Sound Vib 331(7):1686–1700
21. Aydin K (2013) Free vibration of functionally graded beams with arbitrary number of surface cracks. Eur J Mech A Solids 42:112–124
22. Tada H, Paris PC, Irwin GR (1973) The stress analysis of cracks handbook. Del Research Corporation, Hellertown
23. Touloukian YS (1967) Thermophysical properties of high temperature solid materials. McMillan, New York